KEC Conference 2026
ISSN: 3021-940X (Print)
DOI: 10.3126/injet.v3i2.95578

3D Finite Element Analysis of Geogrid-Reinforced Pavement Performance under Heavy Vehicle Loading in a Curved and Graded Highway Section over Weak Subgrade: A Case Study of Bishaltar, Nepal

Prashanna Shrestha[1*], Aanchal Tiwari[2], Ram Chandra Tiwari[3], Prabhat Kumar Jha[4]

[1]*Department of Civil Engineering, Pulchowk Engineering Campus, I.O.E., T.U., Lalitpur, Nepal, Prashannashrestha02@gmail.com*
[2]*Department of Civil engineering, Cosmos College of Management and Technology (CCMT), P. U., University, Kathmandu, Nepal, 079mstre001.aanchal@pcampus.edu.np*
[3]*Department of Civil Engineering, Pulchowk Engineering Campus, I.O.E., T.U., Lalitpur, Nepal, rct2075ce_rctiwari@pcampus.edu.np*
[4]*Ministry of Physical Infrastructure and Transport (MoPIT), Government of Nepal, geoprabhat@gmail.com*

Abstract

The Bishaltar section of Prithvi Highway in Dhading District, Nepal, is a critically distressed pavement segment characterized by combined horizontal curvature (R=40m) and longitudinal gradient (G=4.56%), along with high super elevation (e=6.8%) and a very weak subgrade (california bearing ratio, CBR=2.83%, modulus, $E=2.83\times10^4$ kPa). Despite being designed using IRC and Department of Roads (DoR) guidelines for an 80kN standard axle load and 30 million standard axle (MSA) through IITPAVE software, the pavement has exhibited persistent surface distresses, early rutting, and premature fatigue cracking, often rendering it unrepairable due to recurring structural deficiencies. A detailed 3D finite element analysis using PLAXIS 3D with Mohr-Coulomb material modeling was conducted, incorporating 27 loading phases to simulate the complex stress path induced by a 12-wheeled 33 Ton gross weight truck under curved and upgraded conditions. Results show that geogrid placement at the subgrade-base interface (SB) is most effective for rutting control, achieving service life ratio (SLR) values of 1.576 (vertical compressive strain, ε_{zz}) and 1.588 (Principal compressive strain, ε_1). The combined SB and base-asphalt (BA) configuration provides maximum transverse strain reduction (54.7%, SLR=2.207), whereas BA alone is detrimental, increasing subgrade strain. Geogrid stiffness influence is minimal, with EA=300-600 kN/m identified as performance optimal. The study highlights the limitations of conventional design approaches and underscores the necessity of reinforcement-based design for critical curved and graded highway sections.

Keywords: Geogrid reinforcement, Curvature and gradient, Weak subgrade, Pavement failure, Finite element analysis, Service Life Ratio (SLR), Rutting, Fatigue cracking

1. Introduction

Nepal's road transportation system plays a vital role in national connectivity and economic development, with a strategic road network exceeding 14,000 km managed by the Department of Roads [1]. A significant proportion of these roads are surfaced with flexible pavements due to their lower initial cost, ease of construction, and adaptability to staged development under increasing traffic demands [2]. The design of flexible pavements in Nepal largely follows mechanistic–empirical principles adapted from international standards such as IRC:37 [3] and AASHTO.

Despite these established practices, premature pavement distress—particularly rutting and fatigue cracking-has been widely observed across Nepalese highways. These failures are especially severe in hilly corridors and horizontal curves, such as those along the Prithvi Highway, where complex terrain and loading conditions accelerate pavement deterioration [4]. One such example is observed at Bishaltar, located in Dhading District along the Kathmandu-Mugling section of the Prithvi Highway, where significant pavement distress has been reported, particularly on curved segments subjected to complex traffic loading conditions (Figure 1).

* *Corresponding author*

Conventional pavement design approaches, including IRC:37 [3], are based on simplified assumptions of straight and flat road geometry subjected to vertical, axisymmetric wheel loads. These methods evaluate critical responses such as vertical compressive strain on the subgrade and horizontal tensile strain at the bottom of bituminous layers using layered elastic theory. However, such simplifications neglect the effects of horizontal curvature and longitudinal gradients, which are dominant characteristics of mountainous road networks like Nepal [5].

In reality, vehicles traversing curved and sloped alignments are subjected to complex three-dimensional loading conditions. In addition to the vertical tire load, an outward centrifugal force ($Fc=Mv2/R$) acts on vehicles negotiating horizontal curves. In contrast, tangential traction forces ($Ft=Ma$) develop due to acceleration or deceleration, particularly on combined curvature–gradient sections [6]. These additional forces significantly influence stress–strain responses within pavement layers and can accelerate damage mechanisms such as rutting and fatigue cracking [7].

Despite the critical importance of these loading conditions, there is a lack of comprehensive research addressing pavement performance under realistic three-dimensional moving vehicle loads in Nepal. In particular, limited studies have examined the behavior of geogrid-reinforced flexible pavements under combined curvature and gradient effects. This represents a significant research gap, emphasizing the need for advanced numerical modeling and analysis to develop more reliable and context-specific pavement design methodologies for Nepal

Figure 1. Surface distress and structural deficiencies identified at Bishaltar, Dhading on the Kathmandu-Mugling section of the Prithvi Highway: Location map (L-Figure), Road condition at Bishaltar (R- Figure)

One representative case highlighting these challenges is the Bishaltar section, located in Dhading District along the Kathmandu-Mugling stretch of the Prithvi Highway [8]. This section, characterized by pronounced horizontal curvature combined with longitudinal gradient, has exhibited significant premature distress, including rutting and fatigue cracking. Such behavior underscores the limitations of conventional design approaches when applied to complex terrain and loading environments.

In this context, the present study evaluates the performance of geogrid-reinforced flexible pavements at the Bishaltar section under realistic conditions. The scope of the study includes quantifying the improvement in pavement service life due to geogrid reinforcement through detailed parametric analysis incorporating realistic three-dimensional vehicle loading conditions accounting combined curvature and gradient effects.

However, certain limitations are acknowledged in the present work. The analysis is based on a single pass of heavy vehicle, representing quasi-static loading condition rather than fully dynamic traffic behavior. Additionally, due to computational constraints, the numerical simulation is performed on a limited representative section of the pavement, with the vehicle modeled to move along the center of the left lane only. Despite these limitations, the study provides valuable insights into pavement response under complex loading conditions and establishes foundation for more advanced future investigations.

2. Methodology

The main aim of this study is to establish a robust methodological framework for pavement analysis, rather than to develop a site-specific mitigation model. Bishaltar is used as a representative case study because it reflects common pavement distress and structural deficiencies observed not only at this location but also in other problematic sections of Nepalese highways, particularly along the Prithvi Highway, including Piplamode, Galchhi Height, and Richoktar. The proposed methodology is therefore intended to be generalizable to similar pavement conditions across Nepal, subject to appropriate calibration of local material, loading, and geotechnical parameters where required. Bishaltar section, as shown in Figure 2, is located along the Prithvi Highway in Dhading District, Nepal. This site is characterized by a sharp horizontal curve with a radius of 40 m, the highest super-elevation in the study (e = 6.80%), a 12 m wide carriageway, and the weakest subgrade condition (CBR = 2.83%, E = 2.83 × 10^4 kPa). Due to its geometric and geotechnical conditions, the section is highly susceptible to subgrade rutting, especially under combined curvature and heavy traffic loading effects. The finite element simulation for this site is conducted over 27 loading phases, representing most extensive phase among all selected locations, which reflects longer curvature length traversed by the design vehicle. The weak subgrade combined with significant centrifugal effects from high super-elevation further intensifies pavement distress potential. In contrast, the critical phases for bituminous and asphalt parameters (Phases 15, 17, and 25) indicate the most complex response conditions across all studied sites. All percentage changes is evaluated at their respective critical phases independently. The figure 3 illustrates the methodological framework of the study encompassing site selection, model development, three-dimensional vehicle loading under combined curvature–gradient conditions, parametric analysis of geogrid reinforcement, and post-processing of pavement responses. Table 1 summarizes the complete site parameters for Bishaltar, including its geometric configuration, material properties, and loading conditions, thereby highlighting its critical behavior under realistic traffic and terrain conditions.

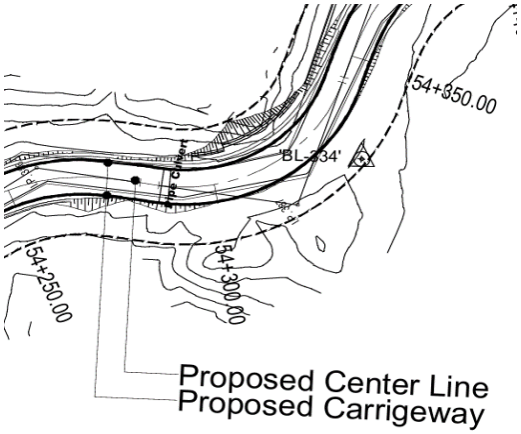

Figure 2. Proposed section of Pavement at Bishaltar, Dhading (54+290-54+350CH) [8]

The moving load simulation was carried out through an automated coordinate generation approach, where the tire path geometry was defined in a curved alignment in accordance with following expressions.

$$x = R * \cos(\theta) \tag{1}$$

$$y = R * \sin(\theta) \tag{2}$$

While the vertical profile was adjusted as:

$$z = f\,(x, y, superelevation, gradient) \tag{3}$$

Equation 3 is used to capture combined effect of cross slope and longitudinal gradient. Dynamic loading was incorporated by considering both centrifugal force Fc and tangential force Ft are respectively follows.

$$Fc = \frac{Mv2}{R} \tag{4}$$

$$Ft = M \cdot a \tag{5}$$

This is done with an initial vehicle speed v_0 =7m/s and acceleration a = 0.5 m/s2. At each loading phase, 12-point loads were activated sequentially to realistically simulate the passage of a moving wheel load along the pavement surface. The linear velocity was converted to angular velocity based on the central turning radius of the vehicle path and the velocity at each phase was updated using the kinematic relationship for accelerated motion, ensuring a realistic time-dependent load progression throughout the simulation. Then, for each loading phase, the corresponding velocity was used to compute the centrifugal force and tangential force every point load along the tire path. Subsequently, the resultant force was decomposed into Cartesian components to be applied at each point load based on its angular position (α) along the curved alignment. The force transformation was carried out as follows:

$$Fx = Fc \cdot cos\ (\alpha) - Ft \cdot sin(\alpha) \quad (6)$$

$$Fy = Fc \cdot sin\ (\alpha) + Ft \cdot cos(\alpha) \quad (7)$$

These resolved force components, together with the vertical load component, were assigned to each of the sequential point loads, ensuring that both magnitude and direction of the moving load system varied realistically with vehicle position along the curvature–gradient section.

The numerical model for the Bishaltar section (CH 54+290 to 54+350) was developed using PLAXIS 3D [9, 10] to simulate a complex road geometry under heavy traffic loading. It utilizes a finite element mesh to analyze soil-structure interaction, specifically evaluating the impact of different geogrid reinforcement configurations on pavement performance (Figure 4) [11-15].

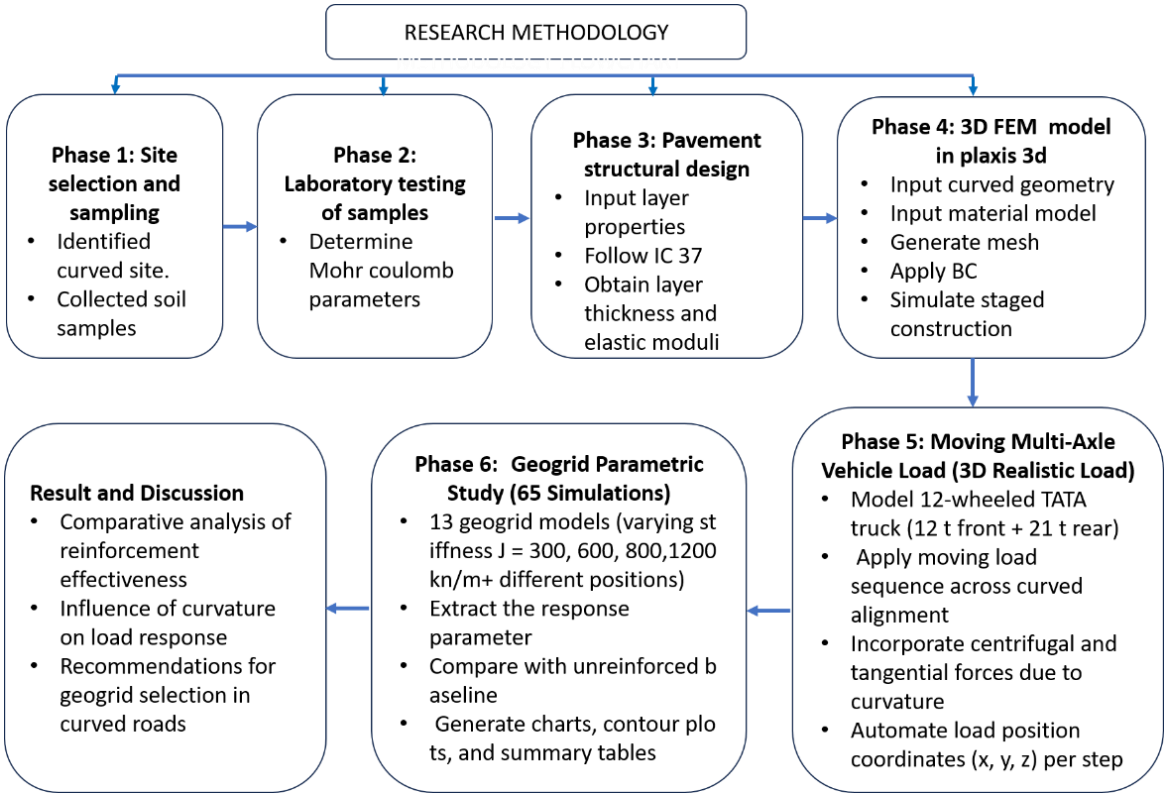

Figure 3. Methodological Framework

Table 1. Site parameters - Bishaltar.

Category	Parameter	Value	Unit / Note
Geometry	Radius of curvature, R	40	m
	Super-elevation, e	6.8	%
	Longitudinal grade, G	4.56	%
	Carriageway width	12	m
	Loading phases	27 (Phase 3–29)	-
Subgrade	CBR	2.83	%
	Unit weight, γ (unsat.)	20.82	kN/m³
	Unit weight, γsat (sat.)	21.25	kN/m³
	Elastic modulus, E	2.83×10^4	kN/m2
	Poisson's ratio, ν	0.35	—
	Effective cohesion, c'	15.6	kN/m2
	Effective friction angle, φ'	45	degrees
	Constitutive model	Mohr-Coulomb (MC)	PLAXIS 3D
Pavement	Surface course	Dense Bituminous Macadam (DBM)	-
	Base course	Water Bound Macadam (WBM)	-
Vehicle	Design vehicle	12-wheeled Tata truck, v_0 =7 m/s, a=0.5 m/s²	-

The finite element mesh was generated in PLAXIS 3D using automatic unstructured 10-noded tetrahedral elements. A mesh sensitivity analysis was conducted, and the final mesh was selected based on a convergence criterion of less than 2% variation in critical strain with further refinement. The local coarseness factors for each soil layer are given in Table 2, following PLAXIS Knowledge Base guidelines [10].

Table 2. Local coarseness factors assigned to each model component.

Layer / Component	Element Type	Local Coarseness Factor	Mesh Density	Justification
Subgrade	10-noded tetrahedra	1.0 (coarsest)	Standard	Diffuse stress zone at depth: coarse mesh is sufficient with minimal accuracy loss.
Granular base course	10-noded tetrahedra	0.75	Medium-fine	Transition zone: moderate mesh refinement captures base–subgrade interaction.
Bituminous asphalt layer	10-noded tetrahedra	0.5	Fine	High stress gradients under tire contact: fine mesh required for accurate strain computation.
Point load locations	10-noded tetrahedra	0.1 (finest)	Very fine	Maximum stress concentration zone; very fine mesh essential for accurate extraction of critical strains

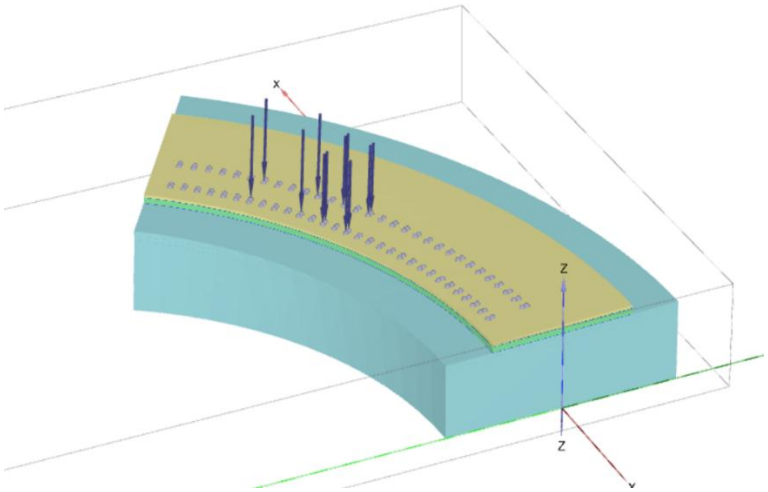

Figure 4. Numerical model of Bishaltar section (54+290-54+350CH) in Plaxis 3D

3. Results and Discussions

The analysis of subgrade response begins with ε_1, representing the minor compressive principal strain at the top of subgrade (ToS), which is a critical indicator for evaluating subgrade rutting potential under traffic loading. The performance is first examined for the case EA = 1600 kN/m, where Phase 11 is identified as the critical loading condition, showing maximum strain response within the simulation domain. Subsequently, the service life ratio (SLR) corresponding to ε_1 is evaluated across all geogrid stiffness values to assess the influence of reinforcement rigidity on subgrade performance. This followed by a comprehensive service life ratio analysis for subgrade rutting parameters, where variation SLR with respect different reinforcement configurations and stiffness levels is systematically compared. The results collectively highlight the sensitivity of subgrade rutting behavior to geogrid stiffness and loading phase, providing a clear understanding of reinforcement efficiency under realistic moving load conditions [11-15].

3.1 ε_1 – Minor Compressive Principal Strain (Top of Subgrade (ToS))

E1 at Bishaltar shares the same critical phase (Phase 11) as Ezz, confirming that rear tandem axle loading at mid-curve is the universally critical loading event for both subgrade rutting parameters at this site. The SLR values for E1 (SLR=1.588 for Subgrade-Base interface (SB) at EA=1600) are slightly higher than for Ezz (1.576), reflecting the additional lateral confinement contribution of the SB geogrid to the principal compressive strain compared to purely vertical Ezz. Base-Asphalt (BA) is adverse for E1 (SLR=0.952–0.953) throughout all stiffness levels. The analysis of the principal strain (E1) at the Top of Subgrade (ToS) for the Bishaltar site demonstrates a clear performance hierarchy across all geogrid stiffness levels. As illustrated in Figure 5, the phase-wise response shows that the SB configuration (green line) consistently maintains the lowest strain levels throughout the loading cycle, while Asphalt-Base (BA) configuration (blue line) consistently stays above "No Geogrid" baseline, indicating a persistent adverse effect. The orange dashed line marks the Critical Phase 11, where the unreinforced pavement experiences its maximum strain; at this vital juncture, the SB layer provides its most significant structural support by absorbing stresses that would otherwise deform the subgrade. This trend is further quantified in Figure 6, which shows the corrected percentage change compared to the unreinforced scenario at the critical phase. The SB interface is the most effective, achieving a peak strain reduction of 37.0% at an axial stiffness (EA) of 1600 kN/m. In contrast, the BA configuration shows a consistent increase in strain of approximately +5.0%, reinforcing the conclusion that placing a geogrid too high in the pavement structure is counterproductive for subgrade protection. While the dual-layer SB+BA setup provides a beneficial reduction of 31.0%, it remains less efficient than the standalone SB layer, suggesting that for this specific road geometry, a single geogrid at the subgrade boundary is the optimal design choice for maximizing pavement longevity.

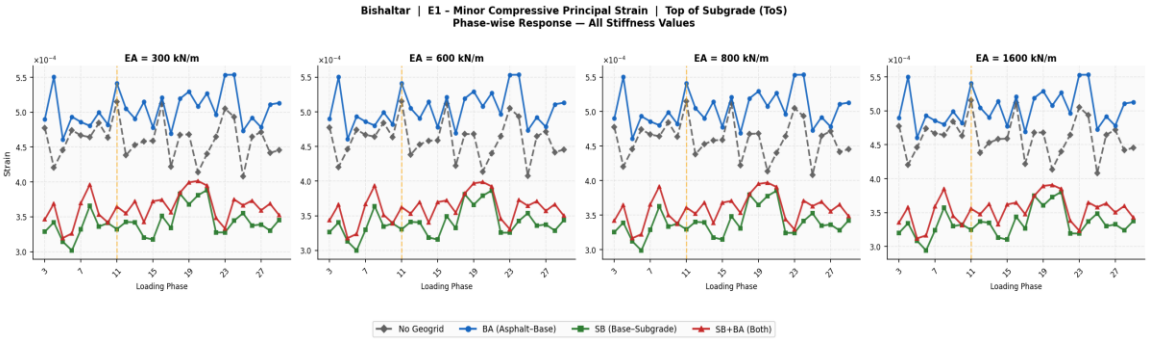

Figure 5. Phase-wise E1 at Top of Subgrade (ToS)-all four stiffness values. Orange-dashed line marks the critical phase for each stiffness level

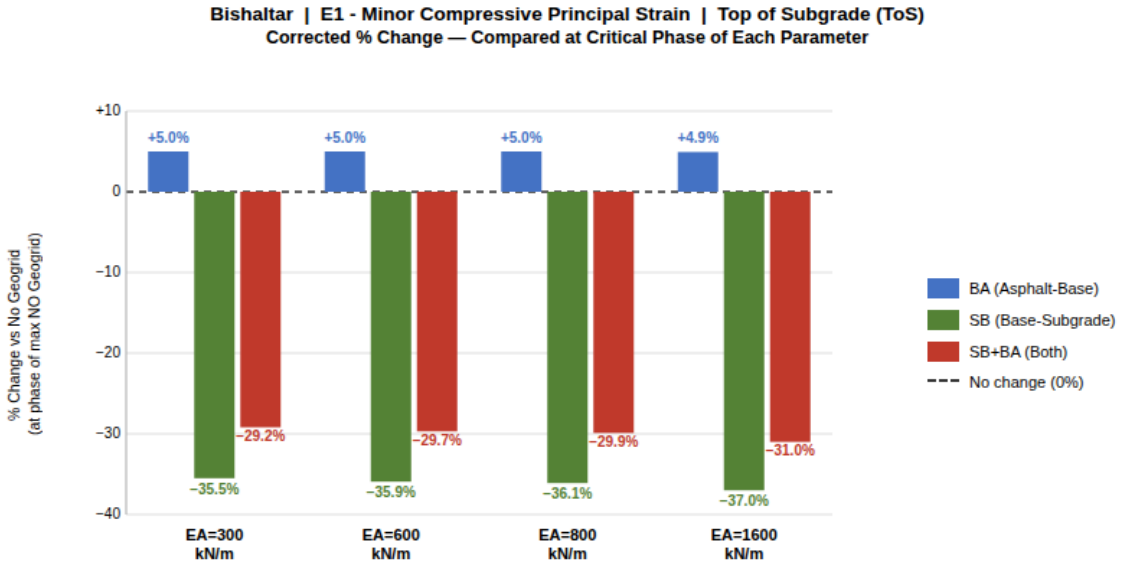

Figure 6. Corrected % change for E1-compared at the critical phase of each stiffness level

3.2 EA = 1600 kN/m (Critical Phase 11)

At EA = 1600 kN/m (Critical Phase 11), the SB configuration exhibits a significant reduction in subgrade response, with a −37.0% change corresponding to an SLR of 1.588 and an approximate life improvement factor of 4.06. The SB+BA configuration also shows improvement, though comparatively lower, with a -31.0% reduction and an SLR of 1.449, indicating a life enhancement of about 2.97. In contrast, the BA configuration has an adverse effect, increasing strain by 4.9% with an SLR of 0.953, confirming its inefficiency under weak subgrade conditions. For comprehensive rutting protection at Bishaltar, the SB geogrid configuration is therefore essential. Notably, the consistency of Phase 11 as the critical phase for both Ezz and E1 responses indicates that a single optimized design specification can effectively address both rutting-related performance criteria simultaneously.

The results for the Bishaltar site at an axial stiffness (EA) of 1600 kN/m, as detailed in Table 3, emphasize that geogrid placement is the most critical factor in mitigating subgrade strain. The SB configuration emerges as the optimal design, achieving a 37.0% reduction in principal strain (E1) at the top of the subgrade. This reduction translates to a Service Life Ratio (SLR) of 1.588 and a significant life extension factor of approximately 8.14. In stark contrast, placement at the BA interface is counterproductive for subgrade protection, leading to a 4.9% increase in strain and a reduction in the relative service life to 0.80. While the dual-layer SB+BA configuration provides a benefit with 5.37 times life factor, it remains less efficient than the single SB layer, indicating that the additional reinforcement at the upper interface may interfere with stress distribution to the subgrade.

Table 3. E1 at EA=1600 kN/m (Critical Phase 11) - Bishaltar. *Life factor = $SLR^{4.53}$ [3]

Configuration	Value at Crit. Phase	% Δ vs No Geogrid	SLR	Life Factor*
No Geogrid (w0)	5.153e-4	-(baseline)	1.000	1.00× (reference)
BA (Asphalt–Base)	5.406e-4	+4.9%	0.953	≈0.80×
SB (Base–Subgrade)	3.245e-4	-37.0%	1.588	≈8.14×
SB+BA (Both Layers)	3.556e-4	-31.0%	1.449	≈5.37×

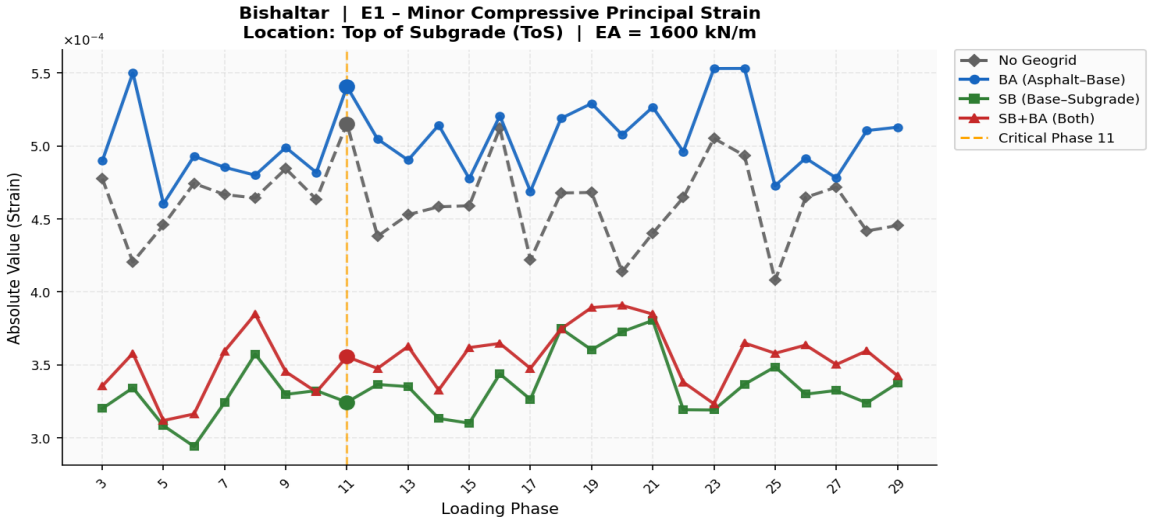

Figure 7. Phase-wise E1 at EA=1600 kN/m. The orange dot at critical Phase 11

Figure 7 further validates these findings by illustrating the phase-wise strain response, where the performance hierarchy remains remarkably consistent across all loading cycles. The green line representing the SB configuration consistently maintains the lowest strain levels. At the same time, the blue line for the BA configuration remains above the "No Geogrid" baseline, signifying a persistent adverse effect. The orange dashed line marks Critical Phase 11, where the unreinforced pavement experiences its peak stress; at this crucial juncture, the SB layer provides its most vital structural support. The visual separation between the green (SB) and red (SB+BA) lines across all phases confirms that for the Bishaltar section, a single geogrid at the subgrade interface is superior to a double-layered approach for controlling subgrade-related failure.

3.3 Service Life Ratio- ε_1 at all stiffness values

The SLR at the critical phase (Phase 11) quantifies the life extension for E1 across all stiffness levels. SLR > 1.0 is beneficial. The SLR is a performance indicator defined as the ratio of allowable to actual strain response, where values greater than 1.0 indicate improved pavement service life under the applied loading.

The data for the Bishaltar site demonstrates that geogrid placement at the SB interface is the most effective configuration for structural reinforcement and life extension. According to Table 4, the SB configuration consistently achieves the highest Service Life Ratio (SLR), reaching a peak of 1.588 at an axial stiffness (EA) of 1600 kN/m, which translates a pavement life extension of approximately 8.14 times compared to unreinforced section. While the dual-layer SB+BA setup is beneficial, it is numerically less efficient than the standalone SB layer, suggesting that adding a second geogrid at the asphalt-base interface may interfere with the stress distribution of the primary subgrade reinforcement. Figure 8 further supports these findings through a percentage change heat-map highlighting a clear trade-off between upper and lower pavement layers. The

SB configuration provides the best subgrade protection with a 37.0% reduction in principal strain (E1), whereas BA configuration is ineffective for the subgrade, actually leading to marginal increase in strain (+4.9%). However, the BA placement excels at reducing horizontal strains at the BoA by 63.2%. Ultimately, both the table and figure confirm that for critical subgrade rutting protection at Phase 11, the SB interface is the optimal choice for this site.

Table 4. SLR at critical Phase 11 - E1-Bishaltar. Dark green SLR ≥ 1.40; light green ≥ 1.10; red ≤ 0.93

EA (kN/m)	Crit. Phase	No Geogrid (at Crit. Ph.)	BA SLR	SB SLR	SB+BA SLR	Life Factor (Best Config)
300	Phase 11	5.153e-4	0.952	1.551	1.413	≈7.31× (SB)
600	Phase 11	5.153e-4	0.952	1.560	1.422	≈7.51× (SB)
800	Phase 11	5.153e-4	0.953	1.566	1.428	≈7.64× (SB)
1600	Phase 11	5.153e-4	0.953	1.588	1.449	≈8.14× (SB)

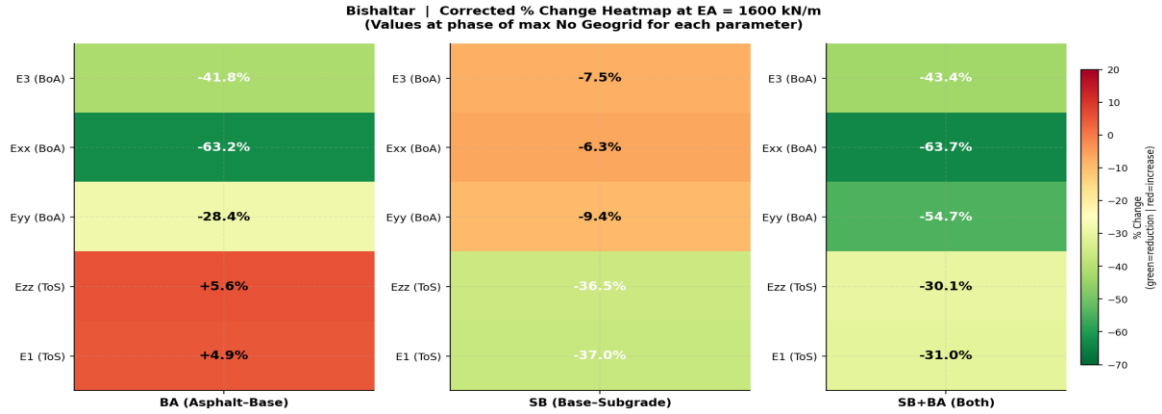

Figure 8. Summary heat map — corrected % change at EA=1600 kN/m for all five parameters × all three geogrid configurations

3.4 Service Life Ratio Analysis -Subgrade Rutting Parameters

The SLR charts below provide a comprehensive view of geogrid effectiveness for subgrade rutting protection at all stiffness levels. SLR = No Geogrid value / Geogrid value at the critical phase. A SLR of 1.50 corresponds to a 33.3% reduction in subgrade strain, according to IRC: 37 [3].

Figure 9 presents the SLR values in a bar chart format, which clearly identifies the (SB) interface as the superior reinforcement location. The green bars consistently outperform the others, maintaining SLR values well above the 1.0 threshold. In contrast, the blue bars for the Asphalt-Base (BA) configuration consistently fall below the dashed line, signifying an adverse effect on subgrade parameters.

Figure 10 utilizes SLR heat-map categorize performance through "benefit-vs-adverse" color scale. The middle horizontal band is entirely green, confirming that the SB configuration comfortably exceeds the 1.50 SLR benchmark-the threshold for a 33.3% strain reduction. Conversely, the top row is highlighted in red, reinforcing the conclusion that placement at the BA interface is detrimental to controlling subgrade strains.

Figure 11 illustrates the linear relationship between geogrid stiffness (EA) and performance. The annotated line chart shows that for both the SB and SB+BA configurations, the SLR improves steadily as stiffness increases from 300 kN/m to 1600 kN/m. However, the chart also reveals a persistent performance gap, where the addition of the BA geogrid in the dual-layer configuration consistently degrades the subgrade protection benefits provided by the SB layer alone.

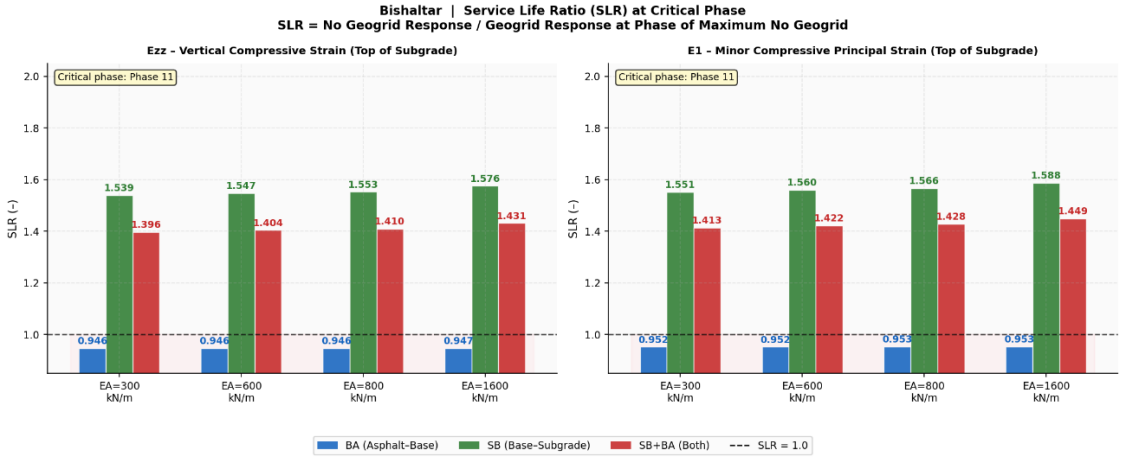

Figure 9. SLR bar chart - BA, SB, and SB+BA at all four stiffness values for Ezz and E1 at their respective critical phases

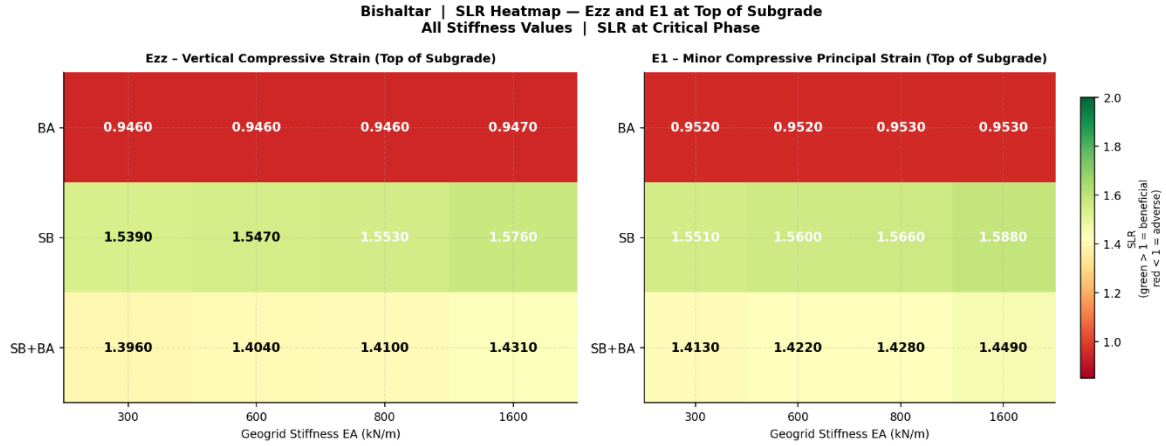

Figure 10. SLR heat map - all configurations × all stiffness values. Green cells indicate substantial beneficial effect; red cells indicate adverse effect

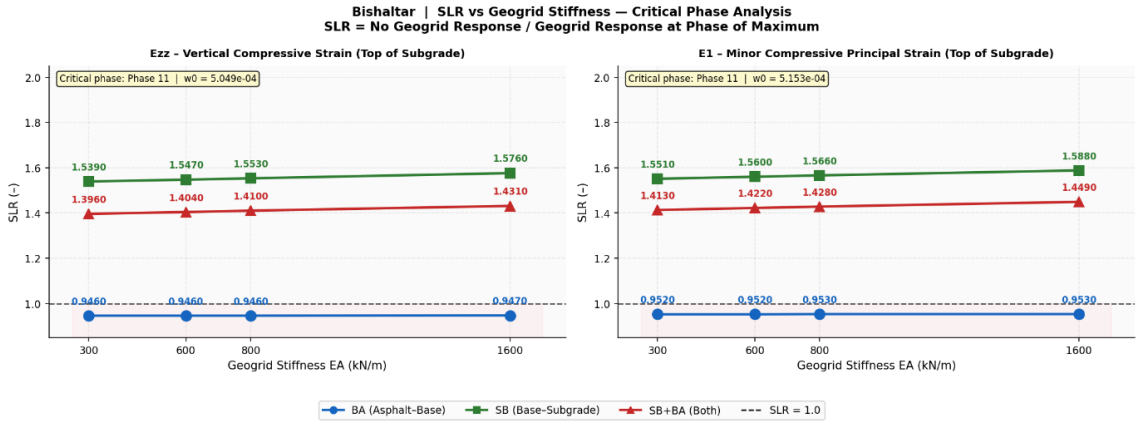

Figure 11. SLR vs geogrid stiffness - annotated line chart showing increasing SLR with stiffness for each

Field validation for the straight section has already been established [16], and the present study extends this validated framework by incorporating centrifugal and tangential forces to realistically simulate vehicle loading effects in the curved section, thereby ensuring the reliability and applicability of the results. Although traffic heterogeneity, temperature variation, and subgrade moisture conditions significantly influence pavement performance on Nepalese highways, a simplified baseline modeling framework has been adopted in this study to establish the methodology under representative conditions. These environmental and traffic variability effects are not explicitly modeled and are clearly acknowledged as limitations of this work.

The present study considers a single-pass static/idealized moving load to capture the immediate pavement response and to establish a clear methodological framework. Dynamic effects such as vehicle-induced vibration, impact loading, and repeated traffic loading cycles are not explicitly included, and therefore long-term distresses such as fatigue cracking and rutting are not directly evaluated.

4. Conclusion

The following conclusions are drawn from the finite element analysis of the Bishaltar section (R = 40 m, e = 6.8%, CBR = 2.83%), located along the Kathmandu-Mugling stretch of the Prithvi Highway:

- **Subgrade–base (SB) configuration is optimal for rutting control**:

The SB configuration provides the most effective reduction in subgrade rutting at Bishaltar, with strain life ratios (SLR) of 1.576 for vertical compressive strain (Ezz) and 1.588 for tensile strain parameter (E1) at EA = 1600 kN/m under the critical loading condition (Phase 11).

- **Combined SB+BA configuration maximizes fatigue resistance:**

The SB+BA configuration achieves the highest reduction in horizontal tensile strain (Eyy), with a 54.7% decrease at the critical Phase 25 (EA = 1600 kN/m), corresponding to an SLR of 2.207. This indicates its effectiveness in enhancing fatigue life of the bituminous layer.

- **Base–asphalt (BA) configuration alone is structurally unfavorable**:

The BA configuration consistently shows adverse effects for both top-of-subgrade (ToS) parameters, with SLR values ranging from 0.946 to 0.953 and an increase in strain of approximately 4.9-5.7%. This represents the most significant adverse BA response among all studied cases and is attributed to the weak subgrade condition (E = 2.83×10^4 kPa), which causes stress concentration beneath the geogrid layer. Therefore, BA reinforcement should not be adopted without SB reinforcement at Bishaltar.

- **Limited sensitivity to geogrid stiffness**:

The influence of geogrid axial stiffness (EA) on pavement performance is relatively low. A stiffness range of EA = 300-600 kN/m is identified as the most cost-effective option across all evaluated performance parameters.

Acknowledgements

The authors sincerely acknowledge Safe and Sustainable Travel Nepal (SSTN) for providing this research opportunity.

References

[1] Department of Roads (DoR), "Strategic Road Network of Nepal," Kathmandu, Nepal: Government of Nepal, 2023.

[2] Department of Roads (DoR), "Guidelines for the Design of Flexible Pavements," Kathmandu, Nepal: Government of Nepal, 2021.

[3] Indian Roads Congress (IRC), *IRC:37-2018 Guidelines for the Design of Flexible Pavements*, New Delhi, India: IRC, 2018.

[4] R. Shrestha and N. K. Tamrakar, "Assessment of flexible pavement performance in hilly roads of Nepal," *Journal of Institute of Engineering*, vol. 15, no. 1, pp. 1–10, 2020.

[5] Y. H. Huang, *Pavement Analysis and Design*, 2nd ed. Upper Saddle River, NJ, USA: Pearson Prentice Hall, 2004.

[6] T. D. Gillespie, *Fundamentals of Vehicle Dynamics*. Warrendale, PA, USA: Society of Automotive Engineers (SAE), 1992.

[7] I. L. Al-Qadi, H. Wang, and E. Tutumluer, "Characterization of flexible pavement response under

moving loads," *Journal of Transportation Engineering*, vol. 134, no. 2, pp. 89–97, 2008.

[8] Department of Roads (DoR), "Proposed Pavement Section at Bishaltar (Chainage 54+290–54+350)," Kathmandu, Nepal: Government of Nepal, 2025.

[9] PLAXIS BV, PLAXIS 3D Scientific Manual — Version 2025.1. Sequent / Bentley Systems, 2025.

[10] PLAXIS Knowledge Base, "Coarseness Factor - Local mesh refinement parameter in PLAXIS 3D," 2015.

[11] N. S. Correia and J. G. Zornberg, "Strain distribution along geogrid-reinforced asphalt overlays under traffic loading," Geotextiles and Geomembranes, vol. 46, no. 1, pp. 111–120, 2018.

[12] N. S. Correia, E. R. Esquivel, and J. G. Zornberg, "Finite-element evaluations of geogrid-reinforced asphalt overlays," Journal of Transportation Engineering Part B: Pavements, vol. 144, no. 2, 04018003, 2018.

[13] J. P. Giroud and L. Noiray, "Geotextile-reinforced unpaved road design," Journal of the Geotechnical Engineering Division, ASCE, vol. 107, no. GT9, pp. 1233–1254, 1981.

[14] H. Wang, I. L. Al-Qadi, and I. Stanciulescu, "Effect of surface friction on tire–pavement contact stresses during vehicle maneuvering," Journal of Engineering Mechanics, ASCE, vol. 140, no. 4, 04014001, 2014.

[15] W. Wang, L. Deng, and X. Shao, "Fatigue life of highway bridges under dynamic impact of heavy trucks," Engineering Structures, vol. 221, 111067, 2021.

[16] A. Tiwari, P. B. Shahi, R. Suwal, and R. C. Tiwari, "Dynamic Analysis of Geogrid-Reinforced Pavement under Area Load Configuration: A Numerical and Field-Based Study" Journal of Transportation System and Engineering, vol. 1(1), 86-102, 2025